Laser-induced magnetization switching in films with perpendicular anisotropy: A comparison between measurements and a multi-macrospin model

C. Bunce,[1] J. Wu,[1,*] G. Ju,[2] B. Lu,[2] D. Hinzke,[3] N. Kazantseva,[1] U. Nowak,[3] and R. W. Chantrell[1]
[1]*Department of Physics, University of York, York YO105DD, United Kingdom*
[2]*Seagate Technology, Recording Media Operations, Fremont, California 94538, USA*
[3]*Fachbereich Physik, Universität Konstanz, 78457 Konstanz, Germany*
(Received 1 July 2009; revised manuscript received 19 April 2010; published 27 May 2010)

Thermally assisted ultrafast magnetization reversal in a dc magnetic field in magnetic multilayer thin films with perpendicular anisotropy has been investigated in the time domain using femtosecond laser heating. The experiment is set up as a stroboscopic optical time resolved magneto-optical Kerr effect magnetometer. It is observed that a modest laser fluence of about 0.3 mJ/cm^2 induces switching of the magnetization in an applied field much less than the dc coercivity (0.8 T) on the subnanosecond time scale. This switching was thermally assisted by the energy from the femtosecond pump pulse. The experimental results are compared with a model based on the Landau-Lifshitz-Bloch equation. The comparison supports a description of the reversal process as an ultrafast demagnetization and partial recovery followed by slower thermally activated switching due to the spin system remaining at an elevated temperature after the heating pulse.

DOI: 10.1103/PhysRevB.81.174428 PACS number(s): 75.50.Ss, 75.40.Mg, 75.40.Gb, 76.60.Es

I. INTRODUCTION

There is currently considerable interest in ultrafast laser-induced magnetization processes. Since the demonstration by Beaurepaire *et al.*[1] that the magnetization can respond to picosecond time scale heat pulses produced by femtosecond lasers, a number of groups[2–4] have studied magnetization processes on this time scale. Experiments generally use pump-probe processes in which a high energy laser pulse is used to heat the sample and a low energy probe pulse (split from the main pulse) is used to monitor the magnetic response using the magneto-optical Kerr effect (MOKE). Much of this work has investigated the dynamics of the destruction and recovery of the magnetization, which can occur on the subpicosecond time scale, although the recovery can take an order of magnitude longer due to frustration effects among large numbers of nucleation sites at which the recovery starts locally.[5]

The dynamics of reversal during a pulsed laser experiment in the presence of an applied field has received less attention. Hohlfeld *et al.*[2] investigated the magnetization reversal induced by 100 fs laser pulses in a GdFeCo magneto-optical recording medium with perpendicular anisotropy. They observed an ultrafast demagnetization of the film occurring within the first picosecond, followed by a slower recovery, taking nearly a nanosecond, in the direction of the applied field as the heat drains from the media layer. They analyzed their measurements using the Bloch equation and concluded that the reversal process was governed by the nucleation and growth of domains in the applied field.

Laser assisted magnetization processes have considerable potential for future ultrahigh-density recording systems. Essentially, the path to higher densities requires a continuous reduction in the grain volume V of the storage medium, necessitating an increase in the magnetocrystalline anisotropy energy density K in order to preserve a sufficiently large value of the parameter KV/k_BT ($\sim$60) to ensure the thermal stability of written information.[6] However, the large value of K impacts the writability of the information, and some scheme is required to overcome this problem. A promising solution is hybrid or heat assisted magnetic recording (HAMR),[7] in which the medium is heated in order to lower the anisotropy and thereby allow information to be written to the medium. Since this is a relatively new field the magnetization reversal mechanisms are not well understood. Although the work of Hohlfeld *et al.*[2] has demonstrated thermally activated domain processes in magneto-optical media, perpendicular recording requires relatively weakly coupled granular media in which domain processes are not the dominant reversal mechanism.

This paper presents time-domain measurements of the magnetization reversal process induced by an ultrafast laser pulse in a thin film with perpendicular anisotropy. The film was especially designed to have a low Curie temperature in order to simplify the experiments. We compare the results with a computational model using the Landau-Lifshitz-Bloch (LLB) equation,[8] which is ideally suited to simulation of magnetization processes up to and beyond T_C and has been shown[9,10] to give an excellent description of the physics of pulsed laser processes. It is concluded that the magnetization response consists of a fast demagnetization followed by a slower response in which the magnetization evolves into the field direction by a process of thermally activated transitions over the local energy barriers. Our LLB-micromagnetic model is shown to give a good description of the physics of the reversal process on both time scales.

II. METHOD

The experiment is a stroboscopic pump-probe experiment using a strong laser pulse to initiate a change in the magnetic state of the sample and a weak probe pulse to observe the resulting magnetization dynamics via the MOKE. The sample is mounted in a spin stand, which first moves the magnetic film through a reset field of magnitude $\sim$1 T for a duration of 0.2 ms which ensures that the sample is in a

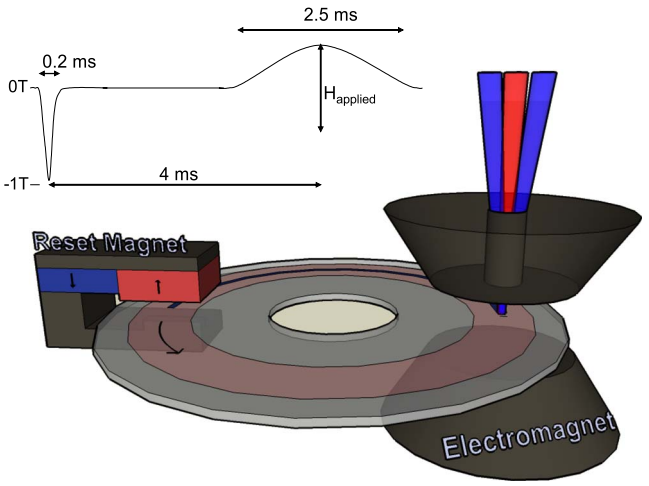

FIG. 1. (Color online) Illustration of spin-stand arrangement used to ensure the materials magnetization is reset between pump pulses.

remanent state before exposure to each laser pulse. Figure 1 illustrates the spin-stand arrangement, with the insert showing the temporal field profile experienced by the magnetic film. After resetting to saturation the sample then moves into a perpendicular applied field by an electromagnet (field range of ± 0.52 T). We note that the field applied is always lower than the static coercivity of the sample as measured at room temperature by a vibrating sample magnetometer. At the center of the pole piece a small hole allows optical access to the sample at which point the sample is exposed to the pump pulse. The laser pulses arrive at a rate of 1 kHz but the rotation of the spin-stand (about 7000 rpm) ensures that freshly saturated film arrives between pulses.

The stroboscopic experiment uses a Libra laser system (made by Coherent) which can produce a 1 kHz stream of 1 mJ, 150 fs pulses of 800 nm radiation. This beam is attenuated, the probe beam is split off and frequency doubled to 400 nm. The pump beam is routed around an optical delay line with 17 fs resolution over a 1 ns range and then focused at normal incidence to a spot approximately 800 μm in diameter on the disk surface. The probe beam is polarized and then brought to a 400 μm focal spot, centered on the pump beam with a power level of about 1/20th of the pump. Because the probe is only half the diameter of the pump it must be noted that there will be a temperature distribution across the region probed. The probe approaches the sample surface at near normal incidence; this polar MOKE geometry yields sensitivity to the out-of-plane component of magnetization. The reflected probe beam is directed into an optical bridge detector, which uses a Wollaston prism to split the beam into two orthogonal polarized components which impinge on a two segment photo-detector. By rotating the detector to the angle where the output of the two polarization channels (A and B) are approximately equal, then the difference between them (A−B) is sensitive to small changes of the polarization angle of the reflected probe which in turn is proportional to m_z. The sum (A+B) is sensitive to changes in reflectivity ΔR, which is associated with temperature changes and stress waves due to processes such as lattice expansions. In order to improve immunity to laser drift the pump beam was chopped and lock-in amplifiers used to detect the sum and difference signals. This makes the measurement sensitive to the difference between the state of the sample without the pump pulse applied and the state induced by the pump pulse. Therefore the measurements are relative and it is difficult to assign an absolute scale to the magnetization changes.

III. EXPERIMENTAL RESULTS

The experiments were conducted on specially prepared samples consisting of CoPt multilayers (Co 0.14 nm/Pt 0.68 nm)$\times 15$ grown on a glass substrate without a soft underlayer. The samples were specifically designed to have a low Curie temperature $T_C=650$ K so that pulsed laser experiments involving temperatures up and beyond T_C could be carried out without damage to the sample. The samples do not have the soft underlayer typical for perpendicular media, but there is 12 nm of seed layer material and a 5 nm capping layer around the media layer (which is approximately 10 nm thick) giving a total film thickness of around 25 nm.

For characterization of the sample the quasistatic hysteresis loop was measured. Of particular importance is the coercivity, which on this time scale is ~ 0.85 T, and the saturation magnetization M_s was measured as 3.2×10^5 A/m. The coercivity of course is already greater than the field applied during our pulsed field experiment. However, it is important to note that the dynamic coercivity on the time scale of the pulsed laser experiment is even larger. The intrinsic coercivity H_0 and the thermal stability factor $KV/k_BT=96$ were measured by making a series of time dependent coercivity measurements and fitting to Sharrock's law.[11] The intrinsic coercivity is related to the anisotropy field and is expected to give a reasonable estimate of the coercivity at the nanosecond time scale. The value of H_0 was found to be 1.4 T; a factor of almost 3 greater than the maximum field available from the electromagnet. The samples have a perpendicular anisotropy K with a value of 3.94×10^5 J/m^3 at room temperatures determined by the rotation method.[12] from which a grain size of 12 nm was estimated.

Figure 2 shows a set of time-resolved measurements on the sample. Figure 2(a) shows the reflectivity data, Fig. 2(b) shows the dynamic magnetic response for zero applied field, and Fig. 2(c) shows the response in the presence of a reversing field of 0.52 T. The laser pulse energy is varied up to 1.14 μJ per pulse (which corresponds to a fluence of approximately 0.23 mJ/cm^2). This value is the largest that can safely be applied to this sample as energy fluences above about 0.5 mJ/cm^2 damage the sample. The sample reflectivity data shown in Fig. 2(a) is a probe of the electron/lattice temperature in the system. It indicates that the same temperature profile is generated each time and that the temperature scales with pulse energy. The reflectivity measurement has three distinct features. Within the first 5 ps is a large peak having a width of 350 fs, which corresponds to the large rise in electron temperature caused by the arrival of the 150 fs laser pulse. The electron system then establishes thermal equilibrium with the lattice which creates the second, rather

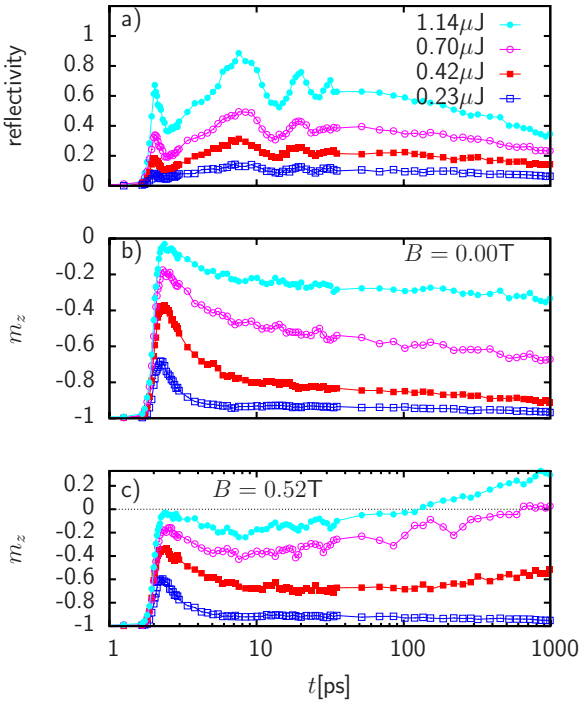

FIG. 2. (Color online) Series of measurements in an applied reversing field of 0.52 T for different laser pulse energies. (a) shows the reflectivity data, (b) shows the m_z component of magnetization, and (c) shows the response in the presence of a reversing field.

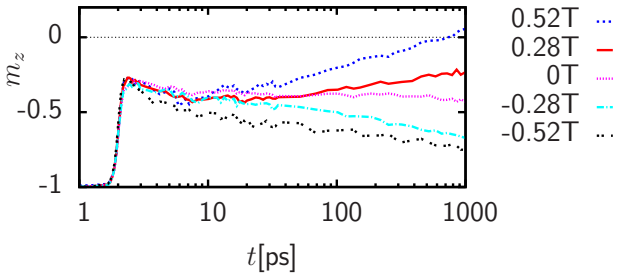

FIG. 3. (Color online) Series of measurements of the temporal variation in m_z in various applied reversing fields for a constant laser pulse energy.

broader, peak 20 ps later. In reality the peak temperature the lattice reaches is much lower than that for the electrons; however, it seems that in this sample the change in reflectivity is more sensitive to the lattice temperature than the electron temperature. The waves seen superimposed onto the lattice temperature peak during the 3–35 ps time frame are probably stress pulses launched into the film by the laser heating of the surface, which reflect off the interface with the glass substrate. The time between peaks is 12 ps, which—given the film and interlayer thickness of 25 nm—suggests a propagation speed of 4100 m/s; consistent with the speed of sound in a typical metal. This complex dependence of the sample Reflectivity on T_e, T_l and other phenomena has been observed by other authors and is, for example, discussed by Djordjevic *et al.*[13] The sample appears to cool rather slowly as the lattice temperature has only fallen to half its peak value after 1 ns. This reflects the fact that in this film there is no heat sink to absorb the heat. Figures 2(b) and 2(c) show the magnetization dynamics in applied fields of 0 and 0.52 T, respectively. Figure 2(c) clearly demonstrates heat assisted reversal due to the pulse. For pulse energies above ~0.5 μJ the sample is seen to cool with the magnetization aligning along the applied field. Recalling that the dynamic coercivity estimated from magnetic measurements is around 1.46 T, this demonstrates a significant heat assistance during the subnanosecond reversal process.

We now consider in detail the processes involved in the magnetization dynamics, which involves three characteristic time scales as illustrated in Fig. 2. The initial phase involves a rapid demagnetization of the sample lagging the change in reflectivity by only 50 fs. The demagnetization takes about 500 fs, independent of the applied field. This is consistent with the normal expectation of a rapid demagnetization as previously demonstrated experimentally[1,2,4] and theoretically.[5,14] The sample then appears to partially recover its magnetization in the original direction, on a time scale independent of the applied field. It is interesting to note that the rate of recovery from the demagnetization peak is inversely related to the amount of demagnetization achieved—a pattern consistent with the calculations of Kazantseva *et al.*[5] Throughout the whole process the only apparent field dependence occurs in the longer time-scale dynamics (20 ps–1 ns). Over this time scale, for the higher laser powers, a gradual reversal of the magnetization is seen.

A similar systematic trend is also exhibited by the temporal variation of m_z at constant laser power in various applied fields, as shown in Fig. 3. The initial disappearance and recovery of the magnetization is similar for all applied fields, but with increasing positive field the long-term trend is clearly toward positive magnetization.

The form of the dynamics, involving a trend against the field direction followed by a slow reversal into the field direction is apparently somewhat counter intuitive. However, the form of the magnetization evolution can be explained by consideration of the different time scales associated with processes at the atomic and macrospin length scales. Within each grain or "macrospin" the disappearance and recovery of the magnetization will be governed by the longitudinal relaxation time, which is temperature dependent but typically of a subpicosecond time scale, which is consistent with the experimental data of Figs. 2(b) and 2(c). However, after this process the system remains at an elevated temperature for around 1 ns, so there is a possibility of thermally activated magnetization reversal. This will have a characteristic time scale determined by the macrospin energy barrier, which is lowered by the reduction of the anisotropy constant at elevated temperature,[15] but typically has values much greater than 1 ps. On this basis we would expect to see a fast reduction and recovery of the magnetization due to atomic processes on the picosecond time scale with a slower relaxation into the field direction due to thermally activated reversal of the macrospins. In order to test this hypothesis in relation to the experimental results we use a computational model of the laser heating process based on the LLB equation, which has been shown[10] to give a good description of magnetization processes over both characteristic time scales.

IV. DYNAMIC MODEL OF LASER HEATING PROCESS

A computational model of laser-induced magnetization dynamics of a thin film with perpendicular anisotropy is used in the following. Consistent with experiments we assume a granular microstructure for the film. For simplicity we assume, in these initial calculations, a monodisperse grain size and anisotropy. Intergranular magnetostatic interactions are included, but the grains are taken as exchange decoupled. As mentioned previously the Landau-Lifschitz-Gilbert (LLG) equation cannot be used for models of laser heating since it does not allow longitudinal fluctuations of the magnetization.[16,17] In the following, we use the LLB equation[8] for the thermodynamic simulation of the laser-induced magnetization switching. As described in detail in Refs. 10 and 18, the LLB equation has been shown by comparison with atomistic calculations to give a remarkably good description of the physics of ultrafast high temperature dynamics. The LLB equation can be written as

$$\dot{\mathbf{m}}_i = -\tilde{\gamma}(\mathbf{m}_i \times \mathbf{H}^i_{\text{eff}}) + \frac{\tilde{\gamma}\alpha_{\parallel}}{m_i^2}[\mathbf{m}_i \cdot (\mathbf{H}^i_{\text{eff}} + \boldsymbol{\zeta}^i_{\parallel})]\mathbf{m}_i$$

$$- \frac{\tilde{\gamma}\alpha_{\perp}}{m_i^2}\{\mathbf{m}_i \times [\mathbf{m}_i \times (\mathbf{H}^i_{\text{eff}} + \boldsymbol{\zeta}^i_{\perp})]\}. \quad (1)$$

Note, that besides the usual precession and relaxation terms in the LLG equation (see Ref. 19 for more details), the LLB equation contains an additional term which controls the longitudinal relaxation. Here, $\mathbf{m}_i$ is a spin polarization which is not assumed to be of constant length and even its equilibrium value $m_e(T)$ is temperature dependent. $\alpha_{\parallel}$ and $\alpha_{\perp}$ are dimensionless longitudinal and transverse damping parameters. Note that $\tilde{\gamma}=\gamma/(1+\lambda^2)$, where γ is the gyromagnetic ratio.

The LLB equation is valid for finite temperatures and even above T_C though the damping parameters and effective fields are different below and above T_C. For $T \leq T_C$ the damping parameters are

$$\alpha_{\parallel} = \lambda\frac{2T}{3T_C} \quad \alpha_{\perp} = \lambda\left(1 - \frac{T}{3T_C}\right) \quad (2)$$

and for $T \geq T_C$ the damping parameters are equal,

$$\alpha_{\perp} = \alpha_{\parallel} = \frac{2\lambda T}{3T_C}. \quad (3)$$

In these equations λ is a microscopic parameter which characterizes the coupling of the individual, atomistic spins with the heat bath.

Thermal fluctuations[20] are included as an additional noise term $\boldsymbol{\zeta}^i_l(t)$ with $l=\perp,\parallel$, $\langle\boldsymbol{\zeta}^i_l(t)\rangle=0$, and

$$\langle\zeta^{i,\nu}_l(0)\zeta^{j,\eta}_l(t)\rangle = \frac{2k_BT}{\tilde{\gamma}\alpha_l M_s^0 \Delta^3}\delta_{\nu\eta}\delta_{ij}\delta(t), \quad (4)$$

where i,j denotes lattice sites and ν,η as the Cartesian components. Here, Δ^3 is the volume of the grains and M_s^0 is the value of the spontaneous magnetization at zero temperature. Note, that these equations are based on the separation of time scales. It is assumed that the heat bath acts much faster than the spin system. Under this assumption the degrees of freedom of the heat bath can be averaged out and replaced by a stochastic field with white noise correlation functions. The prefactor of these functions rests on the fluctuation-dissipation theorem and, therefore, the assumption of white noise is not valid for magnetization dynamics occurring on a time scale comparable to the relaxation time of electron systems (for more details see Ref. 21 and references within.) In our simulations, the electron relaxation time is well above the typical values for electrons in metals and, therefore, the stochastic LLB approach is valid for the treatment of ultra fast reversal processes.

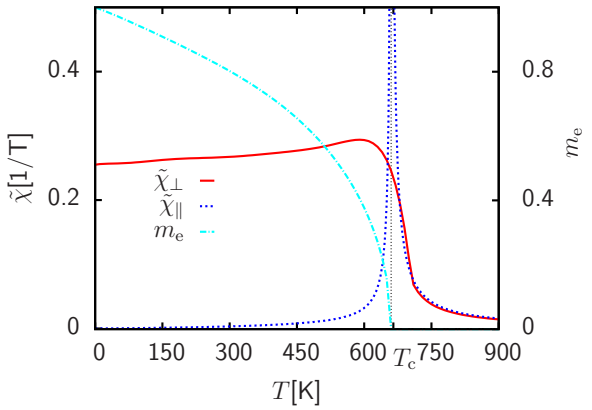

FIG. 4. (Color online) Spontaneous equilibrium magnetization and parallel and transverse susceptibility vs temperature.

The effective fields are $\mathbf{H}^i_{\text{eff}} = -\frac{1}{M_s^0}\frac{\delta f}{\delta \mathbf{m_i}}$, with f as the free-energy density. The total local field is given by[8]

$$\mathbf{H}^i_{\text{eff}} = \mathbf{H} + \mathbf{H}^i_A + \mathbf{H}^i_{\text{dipol}} + \begin{cases} \frac{1}{2\tilde{\chi}_{\parallel}}\left(1 - \frac{m_i^2}{m_e^2}\right)\mathbf{m}_i, & T \leq T_C \\ -\frac{1}{\tilde{\chi}_{\parallel}}\left[1 + \frac{3T_c m_i^2}{5(T - T_c)}\right]\mathbf{m}_i, & T \geq T_C, \end{cases} \quad (5)$$

with the anisotropy field

$$\mathbf{H}^i_A = -\frac{(m^i_x\mathbf{e}_x + m^i_y\mathbf{e}_y)}{\tilde{\chi}_{\perp}}, \quad (6)$$

which makes the z axis the easy axis of the model, and the dipolar field

$$\mathbf{H}^i_{\text{dipol}} = \frac{M_s^0\Delta^3\mu_0}{4\pi}\sum_j \frac{3\mathbf{e}_{ij}(\mathbf{e}_{ij}\cdot\mathbf{m}_j) - \mathbf{m}_j}{r_{ij}^3}. \quad (7)$$

Note that the susceptibilities $\tilde{\chi}_l$ are defined by $\tilde{\chi}_l = \partial m_l/\partial H_l$. At lower temperatures the perpendicular susceptibility $\tilde{\chi}_{\perp}$ is related to the anisotropy K via $\tilde{\chi}_{\perp} = M_s^0 m_e^2/(2K)$.[8] One problem for the application of the LLB equation is that one has to know the functions for the spontaneous equilibrium magnetization $m_e(T)$, the perpendicular $[\tilde{\chi}_{\perp}(T)]$ and parallel $[\tilde{\chi}_{\parallel}(T)]$ susceptibilities.

Here, we use the functions for a generic $L1_0$ material gained from a Langevin dynamics simulation of an atomistic spin model using the material parameters of FePt as de-

scribed in.[18] Although the sample in the experiment is a CoPt multilayer sample, we believe that the simulated material parameters are suitably generic as to be applicable for the multilayer sample used here. We normalize the perpendicular susceptibility in such a way that its value at 300 K is consistent with the experimentally determined values for the anisotropy constant $K=3.94\times10^5$ J/m^3 for our sample. The corresponding input functions are shown in Fig. 4.

The LLB equation is solved numerically by using Langevin dynamics simulations as described in Ref. 19. For our simulations we chose a disk of $32\times32\times1$ cells, with a grain size Δ of 10 nm.

V. COMPARISON BETWEEN MULTI-MACROSPIN MODEL AND EXPERIMENT

In order to make a comparison with the experimental data it is necessary to have an approximation to the temporal variation of the temperature pulse caused by the heating. Because of the complex behavior of the reflectivity as discussed by Djordjevic *et al.*[13] it is not feasible to use this property to directly determine the temperature profile in this work (see Fig. 2 in Ref. 13 for an example of how varied the reflectivity response can be). Instead we make the simplifying assumption that, at low laser powers, the magnetization closely follows the electron temperature during the heating and initial recovery phase; an assumption essentially borne out by calculations in Ref. 5 using an atomistic model, where fast demagnetization and recovery were found for low peak electron temperatures. Following Ref. 5, we assume that the photon energy is transferred to electrons and that the magnetization is directly coupled to the electron temperature T_e within a two-temperature model,[22] expressed as the following coupled differential equations for the electron and phonon temperatures, T_e and T_l, respectively,

$$C_e\frac{dT_e}{dt} = -G_{el}(T_e - T_l) + P(t),$$

$$C_l\frac{dT_l}{dt} = G_{el}(T_e - T_l), \tag{8}$$

where $C_e(T_e)=A_eT_e$ is the electron and C_l is the lattice specific heat, and G_{el} is the electron phonon coupling constant and $P(t)$ is the laser fluence. Equation (8) can easily be solved numerically to generate the time variation in T_e and T_l. We determine the parameters of the two-temperature model by fitting to the form of the initial magnetization decay and recovery. Assuming that the film has a constant temperature distribution created by an absorbed energy fluence of 0.125 mJ/cm^2, then values of $G_{el}=10^{16}$ W/m^3 K, $A_e=60$ J/m^3 K^2, and $C_l=3\times10^5$ W/m^3 K will produce the curves shown in Fig. 5. These numbers represent effective quantities for the Co/Pt layers along with the surrounding seed and capping layers. Although this process cannot be considered an unambiguous determination of these parameters, it is encouraging that the values obtained are comparable to typical values for metals as given elsewhere in the literature, for example see Hohlfeld *et al.*[23]

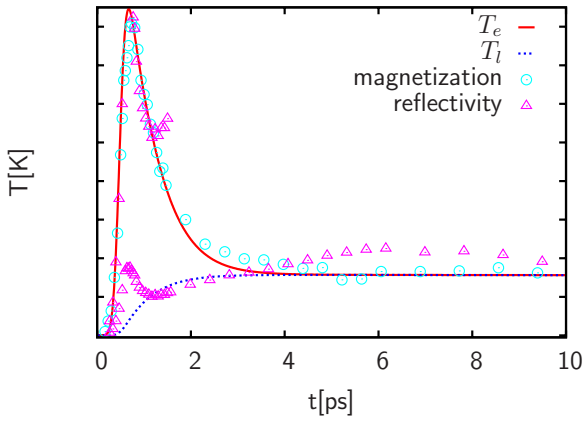

FIG. 5. (Color online) Graph showing the electron temperature (T_e) and the lattice temperature (T_l) simulated by the two-temperature model. Scaled reflectivity and magnetization data are also included for comparison.

Figure 5 shows a comparison of the two-temperature model with the data from the reflectivity and low-laser power magnetization measurements in order to estimate physically reasonable parameters for the model. The time scale of the peak in electron temperature T_e matches the demagnetization peak in the magnetization data and the initial peak in the reflectivity data. The lattice temperature T_l reaches its peak value on the same time scale as the second rise in the reflectivity data. For use in the computational model an interpolation function was fitted to the T_e predicted above. Different laser fluences were simulated by scaling the results to the peak electron temperature (T_e^p), which becomes a main parameter in the comparison with experiment.

Following previous atomistic studies by Kazantseva *et al.*[5] it is clear that the rapid demagnetization observed experimentally can only be achieved if the spin system is coupled to the electron subsystem, which acts as an effective heat bath for the spin system (rather than the lattice) during the laser heating process. As a result our LLB model uses the electron temperature to determine the magnetic properties of the system during the demagnetization process.

In order to obtain close agreement with experiment it is necessary to include an important experimental factor; specifically the fact that the probe pulse area is comparable to that of the pump. This introduces a significant temperature gradient within the probe area, which must be taken into account in the calculations. The effect of this gradient is to enhance the partial recovery effect seen in the measurements. This is because the measured signal is the superposition of the hot material at the center of the probe area (which will be fully demagnetized by the pump heat) and the cooler material at the edge of the pump area which may only partially demagnetize and then recover its magnetization in the original direction. The latter part will effectively give rise to a peak in the demagnetization signal consistent with that observed in the data.

Here, we model this effect using a Gaussian temperature profile for the laser spot. The diameter of the spot used in the model calculations is much smaller than in the experiments (800 μm). This would be an unrealistic approximation if the

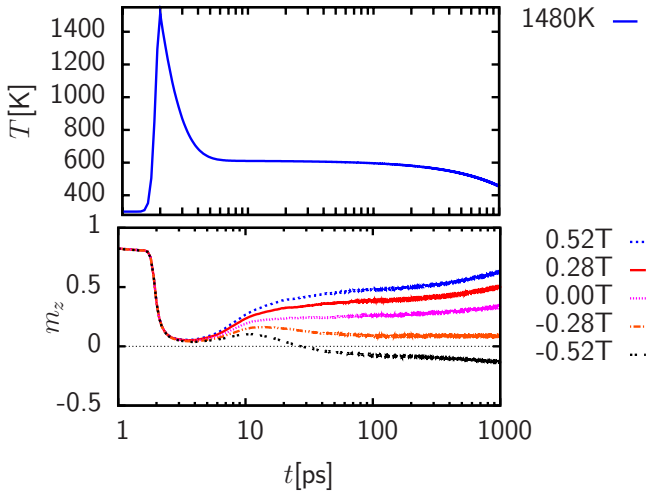

FIG. 6. (Color online) Calculated time dependence of the z component of the magnetization for different applied magnetic fields. $\frac{KV}{k_BT}=95$ with $K=3.94\times10^5$ J/m^3 and $V=(10\text{ nm})^3$ at room temperature ($T_e^p=1480$ K, $\lambda=0.1$).

magnetization reversal involved domain wall processes; however, since the grains are essentially decoupled in the experimental films this simplified model is able to gives some insight into the effects of the temperature profile. Since both pump and probe beams have a Gaussian temperature variation, we take the temperature variation to be of the form $T(r)\propto\exp(-r^2/r_{\text{pump}}^2)$, with r_{pump} as the radius of the pump beam. The MOKE signal is assumed to be proportional to the product of the magnetization and a sensitivity function, proportional to the area generating the signal and the Gaussian weighting, i.e., $\propto m_z r\exp(-r^2/r_{\text{probe}}^2)dr$, with r_{probe} as the radius of the probe. A numerical integration over the probe area was carried out to determine the calculated MOKE signal from the film. The relative ratio of the pump and probe beam diameters effects the shape of the signal measured in the time domain as explained earlier; in the experiment the pump beam was approximately twice the diameter of the probe and in the simulation work it was found that using a probe with a radius of 6.5 cells (to go with a pump radius of 8 cells) gave the best agreement between simulation and measurement.

The model parameters used correspond to an $L1_0$ material with a T_c of 660 K, a M_s^0 of 4.00×10^5 A/m giving a room temperature value of 3.2×10^5 A/m and an out-of-plane anisotropy K of 3.94×10^5 J/m^3 at room temperature. Both values are slightly lower at room temperature than the measured values of our sample. The material is broken up into 32×32 cells of size 10 nm which are exchange decoupled in order to model the granular structure of a recording medium. The intention is to outline the effects of the major parameters in the model, namely the applied field, peak electron temperature and the damping parameter.

Figure 6 shows the temporal response of the magnetization to a laser pulse giving rise to a peak electron temperature of 1480 K assuming a damping parameter λ of 0.1. It can be seen that the simulation gives a reasonable qualitative description of the time evolution of the magnetization following a laser pulse, as shown in Fig. 3. Specifically we note

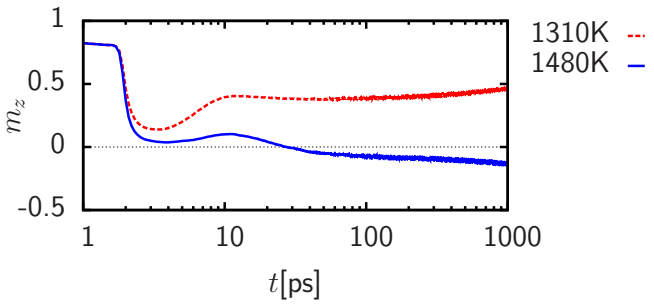

FIG. 7. (Color online) Calculated time dependence of the z component of the magnetization for two different peak temperatures. $\frac{KV}{k_BT}=95$ with $K=3.94\times10^5$ J/m^3 and $V=(10\text{ nm})^3$ at room temperature ($\lambda=0.1$, $B_z=-0.52$ T).

the initial fast demagnetization and recovery. In the case of a positive field the magnetization recovers to the equilibrium value in the positive sense. In a reversing field the initial recovery is followed by a slow reversal of the magnetization toward the field direction which, consistent with the experimental data. The material parameters used for the simulations are in good agreement with the experimentally determined parameters, in particular the room-temperature value of $KV/k_BT=95$ is close to the measured value of 96. It is interesting to note that for larger values of M_s^0 the system appears to lock into a domain state during reversal, which suggests that even at elevated temperatures the intergranular magnetostatic interactions can play an important role. The intergranular exchange coupling can be added, but values as big as 10% of the exchange constant for the material do not change the results significantly. As noted by Kazantseva *et al.*,[5] changes in the value of the damping constant affect the amount of energy the magnetic system absorbs from the initial heat pulse and so how much of a demagnetization is achieved for a given peak electron temperature. In addition there is a slight broadening in the demagnetization peak.

Figure 7 explores the effect of increasing the peak electron temperature. As might be expected, the effect of increasing this parameter is to cause a more complete demagnetization during the laser pulse, and to have a greater net impact on the resulting magnetic state of the sample.

Finally, we consider the effect of the damping parameter λ. Calculations for three different values of λ are shown in Fig. 8. Here, it can be seen that the effect of increasing λ is

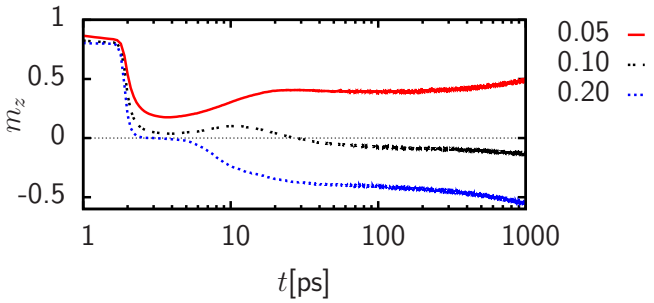

FIG. 8. (Color online) Calculated time dependence of the z component of the magnetization for different values of λ. $\frac{KV}{k_BT}=95$ with $K=3.94\times10^5$ J/m^3 and $V=(10\text{ nm})^3$ at room temperature ($T_e^p=1480$ K, $B_z=-0.52$ T).

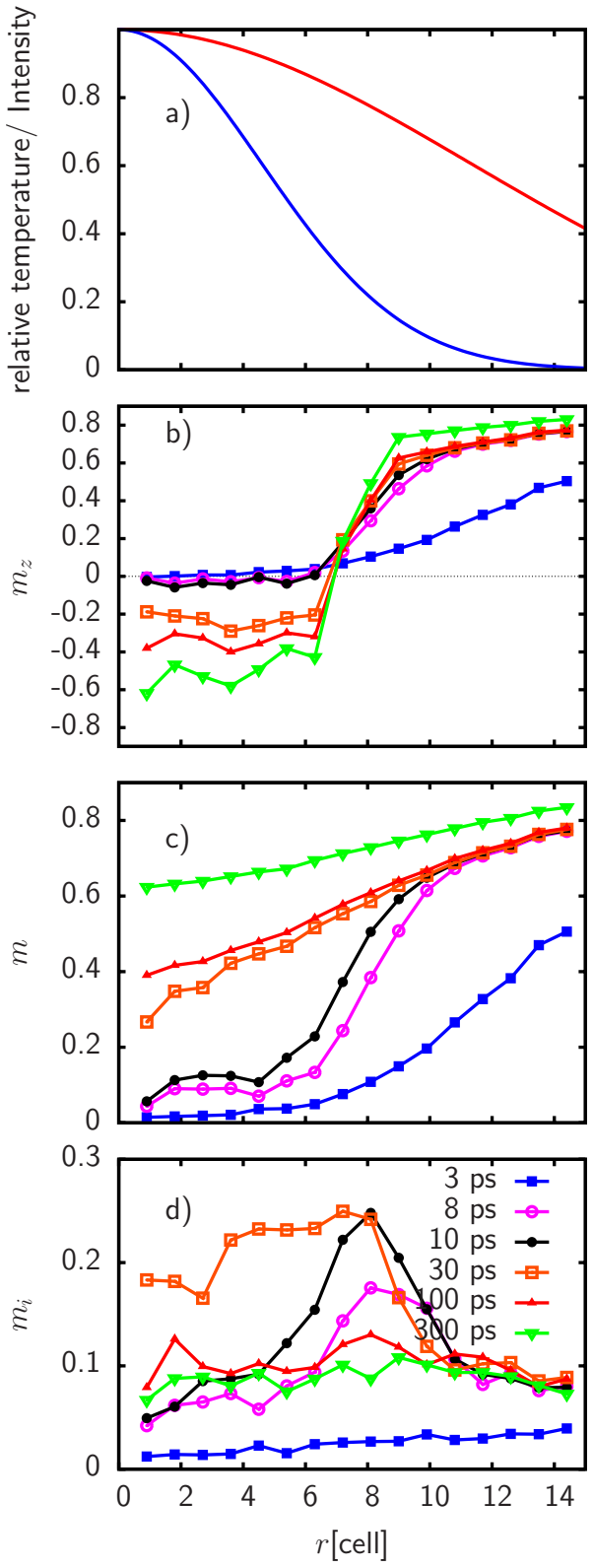

FIG. 9. (Color online) Radial magnetization in a 0.52 T reversing field as a function of time after the laser pulse. Part (a) of the graph shows the relative radial temperature profile (red) and the relative radial intensity of the probe beam (blue). Part (b) shows the perpendicular component m_z, (c) the magnitude m, and (d) the magnitude of the in-plane component m_i.

to achieve a more rapid demagnetization. This is consistent with previous calculations,[5] where the effect is interpreted in terms of the more efficient transfer of energy into the spin system at large λ leading to a more complete demagnetization for a given laser pulse width. Clearly the increased demagnetization caused by the stronger coupling to the conduction electron system results in an increased heat assistance of the magnetization reversal. For the case of $\lambda = 0.05$ it can be seen that too little energy was transferred to fully demagnetize the system. The system has therefore recovered magnetization in the original direction (antiparallel to the applied field) in a similar manner to that seen in Fig. 7 where the lower peak temperature also results in an insufficient demagnetization to achieve reversal.

Figure 9 shows a more detailed analysis of the LLB simulations, indicating that the magnetization dynamics are an ultrafast demagnetization and recovery caused by the electron temperature peak, after which the elevated temperature of the lattice causes a gradual switching of the individual grains of material. Figure 9 shows the temporal evolution of the radial magnetization defined such that $m_\alpha(r)dr$ is the spatially averaged magnetization over the annulus $r \rightarrow r+dr$; here α is the z component of the magnetization m_z [Fig. 9(b)], the total magnetization [Fig. 9(c)], and the in-plane magnetization, defined as the spatial average of $(m_x^2+m_y^2)^{1/2}$ [Fig. 9(d)].

We consider the behavior of two distinct regions; the central region for radius <7 cell radii, where the temperature exceeds T_c during the pulse, leading to complete demagnetization, and the outer region which does not. The variation of the total magnetization [Fig. 9(c)] is consistent with previous calculations.[5] Specifically, the rate of recovery of the magnetization depends upon the magnetic state at the moment of maximum demagnetization. Within the central region the material is completely disordered and the recovery of the magnetization is relatively slow due to the need for the magnetization to recover from highly disordered states. In the outer region the magnetization retains some memory of the initial state, which results in a rapid recovery.[5]

Of most importance in terms of heat assisted reversal is the behavior of the central region. Heat assistance of the reversal is demonstrated clearly in Fig. 9(b), which shows reversal of the central (heated) region while the magnetization in the outer region is not switched. The nature of the reversal in the central region is further investigated using the radially resolved in-plane component of the magnetization, which is shown in Fig. 9(d). It is interesting to note that a large in-plane component develops on the time scale of $10 \rightarrow 30$ ps. This results from the relatively random recovery of the direction of the magnetization after cooling though T_c. This contributes to the magnetization reversal in two ways. First, some of the grains take on a negative sense of the magnetization on recovery. Others will recover in a positive sense but at an angle greater than the energy maximum as the anisotropy increases; these grains are most likely to switch into the negative direction as the temperature decreases. At longer time scale, and consequently lower temperatures, the in-plane component reduces as the magnetization of each grain begins to lie preferentially along the easy anisotropy axis. However, the in-plane component does not completely

disappear, probably reflecting the Boltzmann distribution of the magnetization direction in each grain. In addition to these mechanisms it is also likely that there will be thermally activated reversal over the energy barriers at the elevated temperatures. Along with the increase in spontaneous magnetization as the film cools this would contribute to the gradual reversal over time scales of 1 ns.

VI. CONCLUSIONS

We have presented laser pump-probe measurements, which show a clear heat assistance from the laser pulse for switching the magnetization state. This is demonstrated by the ability to switch in an externally applied field with a magnitude lower than the intrinsic coercivity. The experiments show a rapid demagnetization and recovery followed by a slow evolution of the magnetization into the field direction. This is consistent with the existence of two characteristic relaxation times; the longitudinal and transverse relaxation times. The former involves atomic-scale processes and is typically of the subpicosecond order, whereas the transverse relaxation time reflects transitions over the energy barrier and can be orders of magnitude longer. In order to investigate the reversal mechanism we have developed a micromagnetic model based on the LLB equation which naturally includes both time scales. The LLB model calculations are in good quantitative agreement with the experimental data, as long as the temperature gradient across the probe pulse is included. It appears that on the short time scale (2 ps) there is a rapid demagnetization of m_z due to an associated loss of M_s via the longitudinal relaxation. There is a partial recovery of m_z in the original direction as M_s starts to recover. However, the switching is assisted by the recovery of the magnetization of individual grains in random directions as the system cools through T_c. On the longer time scale the reversal of m_z in the applied field may also be assisted by thermally activated switching caused by the elevated lattice temperature. The elevated temperature has the effect of lowering the anisotropy energy barriers (due to the reduced values of the Magnetocrystalline anisotropy energy) and also provides the thermal energy to induce the transitions. The complex behavior requires a model including both the longitudinal and transverse relaxation times, which is included here using the LLB equation. Our LLB equation-based calculations encapsulate the physics of the heat-assisted reversal process and suggest the LLB equation as a physically realistic model for heat assisted magnetic recording.

ACKNOWLEDGMENTS

The authors would like to acknowledge the Central Laser Facility (CLF) who loaned the laser system used in the project and S. Lepadatu for his assistance in developing the experiment.

*jw50@york.ac.uk

[1] E. Beaurepaire, J.-C. Merle, A. Daunois, and J. Y. Bigot, Phys. Rev. Lett. **76**, 4250 (1996).
[2] J. Hohlfeld, T. Gerrits, M. Bilderbeek, T. Rasing, H. Awano, and N. Ohta, Phys. Rev. B **65**, 012413 (2001).
[3] A. V. Kimel, A. Kirilyuk, A. Tsvetkov, R. V. Pisarev, and T. Rasing, Nature (London) **429**, 850 (2004).
[4] A. V. Kimel, A. Kirilyuk, P. A. Usachev, R. V. Pisarev, A. M. Balbashov, and T. Rasing, Nature (London) **435**, 655 (2005).
[5] N. Kazantseva, U. Nowak, R. W. Chantrell, J. Hohlfeld, and A. Rebei, EPL **81**, 27004 (2008).
[6] D. Weller and A. Moser, IEEE Trans. Magn. **35**, 4423 (1999).
[7] R. E. Rottmayer, S. Batra, D. Buechel, W. A. Challner, J. Hohfield, Y. Kubota, L. Li, B. Lu, C. Mihalcea, K. Mountfield, K. Pelhos, C. Peng, T. Rausch, M. A. Seigler, D. Weller, and X. M. Yang, IEEE Trans. Magn. **42**, 2417 (2006).
[8] D. A. Garanin, Phys. Rev. B **55**, 3050 (1997).
[9] O. Chubykalo-Fesenko, U. Nowak, R. W. Chantrell, and D. Garanin, Phys. Rev. B **74**, 094436 (2006).
[10] U. Atxitia, O. Chubykalo-Fesenko, N. Kazantseva, D. Hinzke, U. Nowak, and R. W. Chantrell, Appl. Phys. Lett. **91**, 232507 (2007).
[11] M. P. Sharrock, J. Appl. Phys. **76**, 6413 (1994).
[12] V. W. Guo, Bin Lu, X. W. Wu, G. Ju, B. Valcu, and D. Weller, J. Appl. Phys. **99**, 08E918 (2006).
[13] M. Djordjevic, M. Lüttich, P. Moschkau, P. Guderian, T. Kampfrath, R. G. Ulbrich, M. Münzenberg, W. Felsch, and J. S. Moodera, Phys. Status Solidi **3**, 1347 (2006).
[14] B. Koopmans, H. H. J. E. Kicken, M. van Kampen, and W. J. M. de Jonge, J. Magn. Magn. Mater. **286**, 271 (2005).
[15] O. N. Mryasov, U. Nowak, K. Y. Guslienko, and R. W. Chantrell, EPL **69**, 805 (2005).
[16] G. Grinstein and R. H. Koch, Phys. Rev. Lett. **90**, 207201 (2003).
[17] V. V. Dobrovitski, M. I. Katsnelson, and B. N. Harmon, Phys. Rev. Lett. **90**, 067201 (2003).
[18] N. Kazantseva, D. Hinzke, U. Nowak, R. W. Chantrell, U. Atxitia, and O. Chubykalo-Fesenko, Phys. Rev. B **77**, 184428 (2008).
[19] U. Nowak, in *Handbook of Magnetism and Advanced Magnetic Materials*, edited by H. Kronmüller and S. Parkin (Wiley, Chichester, 2007), Vol. 2.
[20] D. A. Garanin and O. Chubykalo-Fesenko, Phys. Rev. B **70**, 212409 (2004).
[21] U. Atxitia, O. Chubykalo-Fesenko, R. W. Chantrell, U. Nowak, and A. Rebei, Phys. Rev. Lett. **102**, 057203 (2009).
[22] G. Zhang, W. Hübner, E. Beaurepaire, and J.-Y. Bigot, in *Spin Dynamics in Confined Magnetic Structures I*, edited by B. Hillebrands and K. Ounadjela (Springer-Verlag, Berlin, 2002), p. 245.
[23] J. Hohlfeld, S.-S. Wellershoff, J. Güdde, U. Conrad, V. Jähnke, and E. Matthias, Chem. Phys. **251**, 237 (2000).